

# Astrocytic Tau Deposition Is Frequent in Typical and Atypical Alzheimer Disease Presentations

Amber Nolan, MD, PhD, Elisa De Paula Franca Resende, MD, Cathrine Petersen, BA, Kyra Neylan, BA, Salvatore Spina, MD, Eric Huang, MD, PhD, William Seeley, MD, Zachary Miller, MD, and Lea T. Grinberg , MD, PhD

## Abstract

Typical Alzheimer disease (AD) features an amnesic syndrome that reflects the progression of pathology through specific neural networks. However, a subset of patients exhibits atypical onset with prominent language, behavioral, or visuospatial deficits that are not explained by current neuropathological staging schemes. Astroglial pathology featuring tau inclusions with thorn-shaped and granular fuzzy morphologies is common in the aging brain and collectively known as aging-related tau astroglial pathology (ARTAG). Prior studies have identified tau-positive thorn-shaped astrocytes in the white matter that associate with a primary progressive aphasia phenotype in an AD cohort. However, a possible contribution of ARTAG copathology to AD clinical heterogeneity has yet to be systematically examined. To investigate whether ARTAG pathology contributes to atypical presentations, we mapped the presence and density of ARTAG subtypes throughout cortical and subcortical regions in a well-characterized cohort of AD cases enriched for atypical presentations. In our cohort, ARTAG pathology is frequent and correlates with older age and higher Braak stage. ARTAG subtypes exhibit distinct distribution patterns with subpial and subependymal deposition occurring in the amygdala, while white and grey matter astrocytic deposition are distributed throughout cortical regions. However, ARTAG pathology is equally prevalent in cases with typical and atypical clinical presentations.

**Key Words:** Aging-related tau astroglial pathology (ARTAG), Astrocytes, Atypical Alzheimer disease, Clinical heterogeneity, Tau.

From the Department of Anatomic Pathology, University of California, San Francisco, CA (AN, EH, WS, LTG); Memory and Aging Center (EDPFR, CP, KN, SS, WS, ZM, LTG), University of California, San Francisco, California; and Global Brain Health Institute based at University of California, San Francisco and Trinity College, Dublin, Ireland (EDPFR, LTG).

Send correspondence to: Lea T. Grinberg, MD, PhD, Memory and Aging Center, University of California, San Francisco, 675 Nelson Rising Lane, San Francisco, CA 94158; E-mail: lea.grinberg@ucsf.edu

Amber Nolan and Elisa De Paula Franca Resende contributed equally to this work.

This work was supported by the following research grants: NIH Grant K24AG053435, and institutional NIH Grant P01AG019724, P50AG023501. The authors have no duality or conflicts of interest to declare.

[Supplementary Data](#) can be found at [academic.oup.com/jnen](http://academic.oup.com/jnen).

## INTRODUCTION

The typical clinical presentation of Alzheimer disease (AD) features an evolving amnesic syndrome thought to reflect the progression of pathological changes through specific neural networks (1, 2). However, a subset of patients exhibits an atypical clinical onset with prominent motor, language, behavioral, or visuospatial deficits that have been termed “focal cortical presentations.” These include corticobasal syndrome, primary progressive aphasia, especially the logopenic variant, posterior cortical atrophy, and behavioral variant/dysexecutive syndrome (2–9). Despite this variability in clinical presentation, current neuropathological staging schemes (i.e. CERAD, Thal, and Braak) fail to explain this clinical heterogeneity (2, 10). The presence of additional copathologies has been hypothesized to contribute to focal cortical archetypes in AD. For example, some evidence suggests that coexisting Lewy body pathology may increase perceptual impairment and contribute to a posterior cortical atrophy syndrome (2, 11), while coexisting vascular pathology in the frontal lobes may exacerbate executive dysfunction (2).

Astrocytic inclusions composed of hyperphosphorylated tau protein in different shapes and locations frequently appear in the aging brain (12–17). To enable systematic studies on the role of tau astroglial pathology, an international group of neuropathologists proposed guidelines for classifying these astrocytic lesions under the terminology of aging-related tau astroglial pathology (ARTAG) (12). Thorn-shaped (TSA) and granular-fuzzy astrocytic (GFA) inclusions represent the two main ARTAG morphologies and exhibit differential patterns of deposition. TSAs deposit in subependymal, subpial, perivascular, white matter and grey matter regions, whereas GFAs are limited to the grey matter. The clinical impact of ARTAG is poorly understood, but some studies suggest a potential role for ARTAG in lowering the threshold for dementia or contributing to focal cortical symptoms (18, 19). In particular, Munoz et al found that 7/8 cases of primary progressive aphasia displayed prominent TSAs at the grey-white junction in cortical areas, whereas a similar number of amnesic AD cases had none (18). However, very few studies have examined ARTAG distribution and frequency outside the temporal lobe in well-characterized clinical AD cohorts. Moreover, ARTAG has yet to be explored as a possible determinant of atypical presentation in AD.

We took advantage of a large clinicopathological cohort of AD cases lacking any comorbid cortical pathology to systematically map ARTAG throughout several cortical and subcortical brain regions. Both classical logistic regression and unbiased clustering techniques were used to investigate whether co-existing ARTAG, by subtype and location, correlates with a focal cortical presentation of AD.

## MATERIALS AND METHODS

### Participants

All studies were approved by the UCSF institutional review board. All participants were part of the clinicopathological cohort of the Neurodegenerative Brain Bank of the Memory and Aging Center at the University of California, San Francisco (UCSF). Each individual underwent an in-depth neurological history, examination and comprehensive neuropsychological and functional assessment including the Clinical Dementia Rating (CDR) at least once. Also, at the time of autopsy, an extensive postmortem assessment covering dementia-related function was performed with the family. Neuropathological diagnosis followed currently accepted guidelines (20–24); subtyping for FTLT-DTP and FTLT-tau followed the current “harmonized” nomenclature (25, 26).

The cases for this study included those with a primary neuropathological diagnosis of AD neuropathological change procured by the Neurodegenerative Disease Brain Bank between 2008 and 2016, while excluding those with co-occurring frontotemporal lobar degeneration (FTLT-FUS, tau, or TDP-43 primary pathology), chronic traumatic encephalopathy (CTE), hippocampal sclerosis,  $\alpha$ -synuclein pathology staged Braak  $\geq 3$  or contributing cerebrovascular lesions, leading to a total of 83 cases for analysis. Argyrophilic grain disease (AGD) was not a criterion for exclusion based on its high prevalence and lack of correlation with significant clinical symptoms (27–29).

### Additional Immunohistochemistry

Eight  $\mu$ m-thick sections of tissue were cut from formalin-fixed and paraffin-embedded tissue blocks from the anterior cingulate cortex, middle frontal gyrus, inferior frontal gyrus (pars opercularis), insula, angular gyrus, and entorhinal cortex as well as the amygdala and putamen. These cortical sections were chosen to represent areas showing a discrepant pattern of atrophy in atypical AD cases. These sections were immunostained against a hyperphosphorylated tau antibody (CP-13, Ser202; 1:500, gift from Dr. Peter Davies, Albert Einstein College of Medicine) and counterstained with hematoxylin for evaluation. All analyses and neuropathological evaluations were performed while blinded to the clinical diagnosis.

### Evaluation of Tau Pathology

Astrocytic tau deposits were classified according to the recent harmonized evaluation strategy (12). TSAs were identified by the prominent eccentric somatic tau deposition and were found in white matter, grey matter, perivascular, subpial, and subependymal locations. GFAs were recognized as cells

with abundant granular deposition in astrocytic processes forming bush-like or starburst-like patterns, and were only found in grey matter. The presence or absence of these astrocytic morphologies in each compartment (white matter, grey matter, subpial, subependymal, perivascular) within each region of interest listed above was determined. Also, to gain a semiquantitative approximation of the ARTAG pathology density present, the area of highest density within each compartment per slide was identified by the evaluating neuropathologist (A.N.), and a count of the number of astrocytes with tau inclusions present within a 20 $\times$  objective microscopic field was quantified. Regarding nomenclature, the term ARTAG refers to the presence of TSA or GFA inclusions in any location. Furthermore, we often denote the presence of TSAs in the white matter (which almost exclusively occur at the grey-white junction) as argyrophilic thorny astrocyte clusters (ATAC), given the association of this specific pathology to language presentation with AD pathology (18).

The hippocampus, inferior frontal cortex, and the amygdala were also evaluated for AGD. The presence of AGD was determined by having 3 of 4 criteria in the hippocampus (1: grains, 2: coiled bodies, 3: eyeliner sign in CA2, and 4: tau inclusions in the dentate) and the presence of grains and coiled bodies in the amygdala or inferior temporal cortex; these criteria are stringent and conservative and correspond to at least a stage II of disease as proposed by Ferrer et al (27).

### Clinicopathologic Variables

The clinical syndrome was determined by chart review based on published criteria for typical Alzheimer amnesic syndrome (30–32), posterior cortical atrophy (8, 33), logopenic variant primary progressive aphasia (34), corticobasal syndrome (35), behavioral variant frontotemporal dementia (FTD) syndrome (36, 37), and Lewy body dementia (22). All the charts were reviewed by a behavioral neurologist (E.R.) blinded to the neuropathological status. If any discrepancies were noted in the diagnosis at different points in time or in different evaluations in the chart or if there were any atypical clinical features, the chart was reviewed by a second expert behavioral neurologist (Z.M.), and the final diagnosis was determined after consensus. One patient presented with rapid cognitive decline, hyper-somnolence, parkinsonism, and ataxia and was classified as dementia without other specification because it did not fit any of the clinical syndromes described above. Although the complete CDR was obtained in each visit, for this study, we used the score obtained from an informant from our postmortem evaluation to reflect the functional status around 3 months before death. A diagnosis of very mild dementia required a CDR score of 0.5, and all cognitively normal participants had a CDR of 0 in this evaluation.

In addition to clinical diagnosis, the following variables were obtained from the Memory and Aging Center Clinical Database: Age at death, sex, years of disease duration, years of education, *Apolipoprotein E4 (APOE4)* carrier status, and the Braak stage of AD neuropathological changes related to neurofibrillary tangle accumulation. *Apolipoprotein E* allele genotyping was performed using a TaqMan Allelic Discrimination Assay on an ABI7900HT Fast Real-Time polymerase

chain reaction system (Applied Biosystems, Foster City, CA). A history of head injury was not available for many cases and not included in the analysis at this time.

## Statistical Analysis

Statistical analyses were performed using R Statistical Software (version 3.3.3; R Foundation for Statistical Computing, Vienna, Austria). A Chi-square test or Mann-Whitney *U* test was used to analyze associations between variables of interest (including relationships between pathology subtypes and demographics of pathological groups). A one-way ANOVA with Tukey post hoc examination was assessed to compare regional densities of astrocytic tau deposition. Multivariate logistic regression evaluated the relationship between overall pathology presence and clinical characteristics, accounting for age of death, disease duration, sex, atypical diagnosis, Braak stage, presence of AGD and *APOE4* carrier status. *p* values < 0.05 were considered statistically significant.

Unbiased clustering of the density of ARTAG pathology was also performed to examine how unique pathological groups of astrocytic tau deposition might correlate with clinical variables. A K-means clustering algorithm, which optimizes the sum of the square Euclidean distance between points was chosen. To validate the clustering results, connectivity within a cluster, silhouette width and Dunn's index (factors representing distance within and between clusters) were assessed using the Cluster Validation Package *clValid* in R. The similarity of K-means clustering and Ward's method of partitioning was also evaluated to appraise the robustness of the clustering.

## RESULTS

### Demographics

Table 1 summarizes the clinical characteristics of the 83 cases. Approximately 30% (26/83) of the cohort manifested an atypical clinical presentation including corticobasal syndrome, behavioral variant frontal temporal dementia/dysexecutive syndrome (FTD), logopenic variant of primary progressive aphasia, or posterior cortical atrophy syndrome. The cohort was highly educated and included a higher percentage of men.

### Qualitative Analysis: Morphology, Frequency, and Relationships of ARTAG Subtypes

Astrocytic tau deposition in the white matter (also known as ATAC) occurred either as focal clusters (Fig. 1A) or diffusely paved the grey-white junction (Fig. 1B) and featured a homogeneous thorn-shaped morphology as previously reported (18 (TSA, Fig. 1C). TSAs in the grey matter also appeared in clusters or were diffusely distributed. The density was noted to be higher in the sulcal depth in several cases (6% of total cases, 9% of cases with grey matter TSAs; Fig. 1D–F, Table 2). In contrast, GFAs in the grey matter were often present diffusely and scattered throughout the cortex at a relatively low density (Fig. 1G–I). Both focal and diffuse distributions were noted for subpial and subependymal TSA deposition (Fig. 2A–F). Subpial clusters were often identified

at the sulcal depth as well (11% of total cases, 17% of cases subpial TSAs; Fig. 2A; Table 2). In the amygdala, ARTAG in the white matter was always adjacent to the temporal horns of the lateral ventricle, and thus, astrocytic tau deposition was always categorized as subependymal in this location (Fig. 2D–F). Perivascular TSA deposition was noted around large vessels adjacent to the basal ganglia, insula, and amygdala. In cortical sections, perivascular TSAs often occurred within a larger ATAC cluster in the white matter, and it was only independently included in further analysis if an obvious accentuation around the vasculature was noted (Fig. 2G–I). Despite occasional noting of sulcal accentuation of grey matter and subpial TSAs, we did not find clear perivascular accentuation of astrocytic tau or neuronal tau pathology at the sulcal depth to suggest a diagnosis of CTE.

Concerning prevalence, the presence of any ARTAG type occurred in 64% of cases overall. The most commonly identified ARTAG subtype was TSAs in the white matter (also known as ATAC), identified in almost half of the cohort (47%). The remaining subtypes—grey matter TSAs, grey matter GFAs, subpial, subependymal, and perivascular TSAs—were noted at frequencies between 19% and 36% with GFAs occurring least often. The frequency of pathology by clinical diagnosis, including the sulcal accentuation identified in grey matter and subpial TSAs, is given in Table 2. The frequency of overall ARTAG pathology, ARTAG subtype, or sulcal accentuation in grey matter TSA or subpial TSA groups was not significantly different when comparing each clinical diagnosis to the amnesic or classical AD group (Table 2).

Although ARTAG subtypes are grouped under the same umbrella term, it is unclear if they share similar pathogenesis or etiology. A tendency to accumulate different ARTAG subtypes in the same brain could point to a shared disease mechanism, whereas a tendency of a subtype to occur in isolation may indicate that each subtype represents a different disease process. Thus, we next investigated whether ARTAG subtypes are likely to occur together in the same case, or not (Table 3). We found that cases with ATAC pathology had a significant likelihood (ranging from ~30% to 60%) of also exhibiting another ARTAG subtype. Similar findings were noted for all other subtypes with a range of co-occurring paired pathologies between ~30% and 85%. All pairs of co-existing pathology exhibited a significant relationship (for all relationships *p* < 0.03, Chi-square test; see Table 3 for exact *p* values).

### Semiquantitative Analysis: Density and Distribution of ARTAG

Previous investigations focusing on ARTAG failed to identify a consistently significant clinical correlate outside of age and sex. However, these studies were rather qualitative in nature. Therefore, in addition to the qualitative assessment of the presence or absence of pathology in each section, we also quantified ARTAG density by recording the highest density for each subtype in each location in every slide examined. The anatomic distributions by density for each subtype when present are presented in Figure 3. When TSAs occurred in the white matter (also known as ATAC), the density of pathology was similar throughout all regions of interest (*p* = 0.95,

**TABLE 1.** Demographic Characteristics by Clinical Diagnosis

| Clinical Diagnosis                            | Number | % Male | Mean Age of Death (SD) | Mean Disease Duration (SD) | Mean Years of Education (SD) | %APOE4 carrier | Median Braak NFT stage |
|---|--------|--------|------------------------|----------------------------|------------------------------|----------------|------------------------|
| Amnesic syndrome                              | 46     | 76     | 72.91 (11.31)          | 9.93 (2.86)                | 15.48 (4.11)                 | 55             | 6                      |
| Corticobasal syndrome                         | 7      | 43     | 69.29 (9.30)           | 9.29 (3.30)                | 16.14 (3.08)                 | 29             | 6                      |
| Behavioral variant frontotemporal dementia    | 5      | 80     | 66.20 (4.82)           | 15.00 (4.74)               | 15.67 (3.79)                 | 40             | 6                      |
| Lewy Body Dementia                            | 1      | 0      | 87.00 (–)              | 2.00 (–)                   | 17.00 (–)                    | –              | 2                      |
| Logopenic variant primary progressive aphasia | 7      | 43     | 65.86 (6.26)           | 10.29 (2.06)               | 15.57 (2.30)                 | 33             | 6                      |
| Very mild dementia                            | 7      | 29     | 82.71 (4.82)           | 7.57 (3.41)                | 16.43 (2.94)                 | 29             | 3                      |
| Cognitively normal                            | 3      | 100    | 85.33 (15.31)          | –                          | 15.00 (1.73)                 | 67             | 4                      |
| Other   | 1      | 100    | 66.00 (–)              | 8.00 (–)                   | 16.00 (–)                    | 100            | 6                      |
| Posterior cortical atrophy                    | 6      | 17     | 64.67 (6.52)           | 9.83 (3.92)                | 16.00 (1.67)                 | 0              | 6                      |
| Total   | 83     | 63     | 72.37 (10.96)          | 9.89 (3.45)                | 15.68 (3.45)                 | 45             | 6                      |

SD, standard deviation; NFT, neurofibrillary tangle.

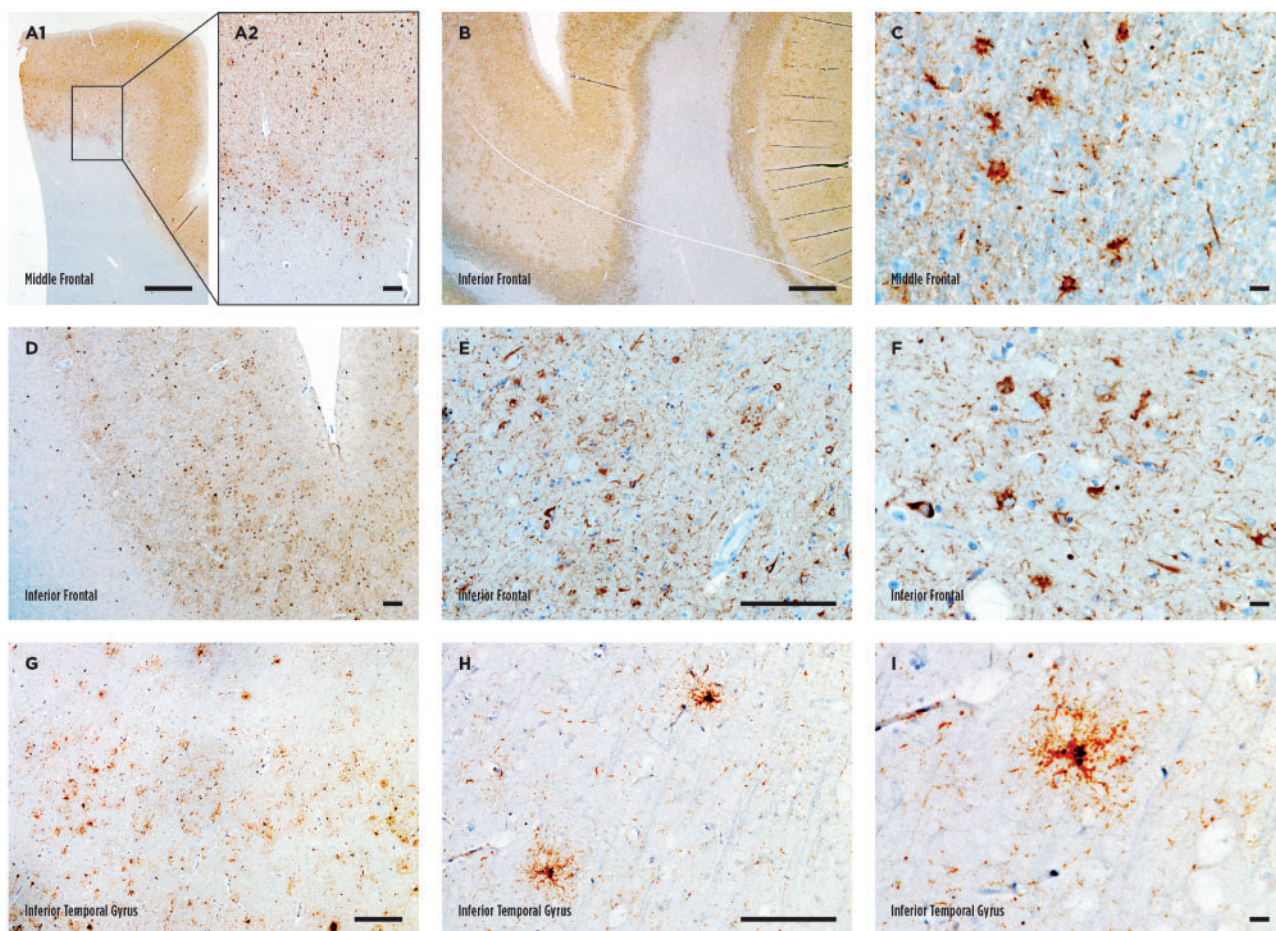


**FIGURE 1.** Astrocytic tau deposition in the white and grey matter. **(A–C)** Representative images of thorn-shaped astrocytes (TSAs) in the white matter visualized with phosphorylated tau immunostaining. An example of a focal cluster is depicted in **A**, while diffuse deposition is shown in **B**. **(D–F)** Representative images of TSA in the grey matter in the inferior frontal gyrus. Notice the sulcal accentuation in panel **D**. **(G–I)** Representative images of granular fuzzy astrocytes (GFA) in the inferior temporal gyrus. Scale bars: **A1, B**, 1000  $\mu\text{m}$ ; **A2, B, D, E, G, H**, 100  $\mu\text{m}$ ; **C, F, I**, 10  $\mu\text{m}$ .

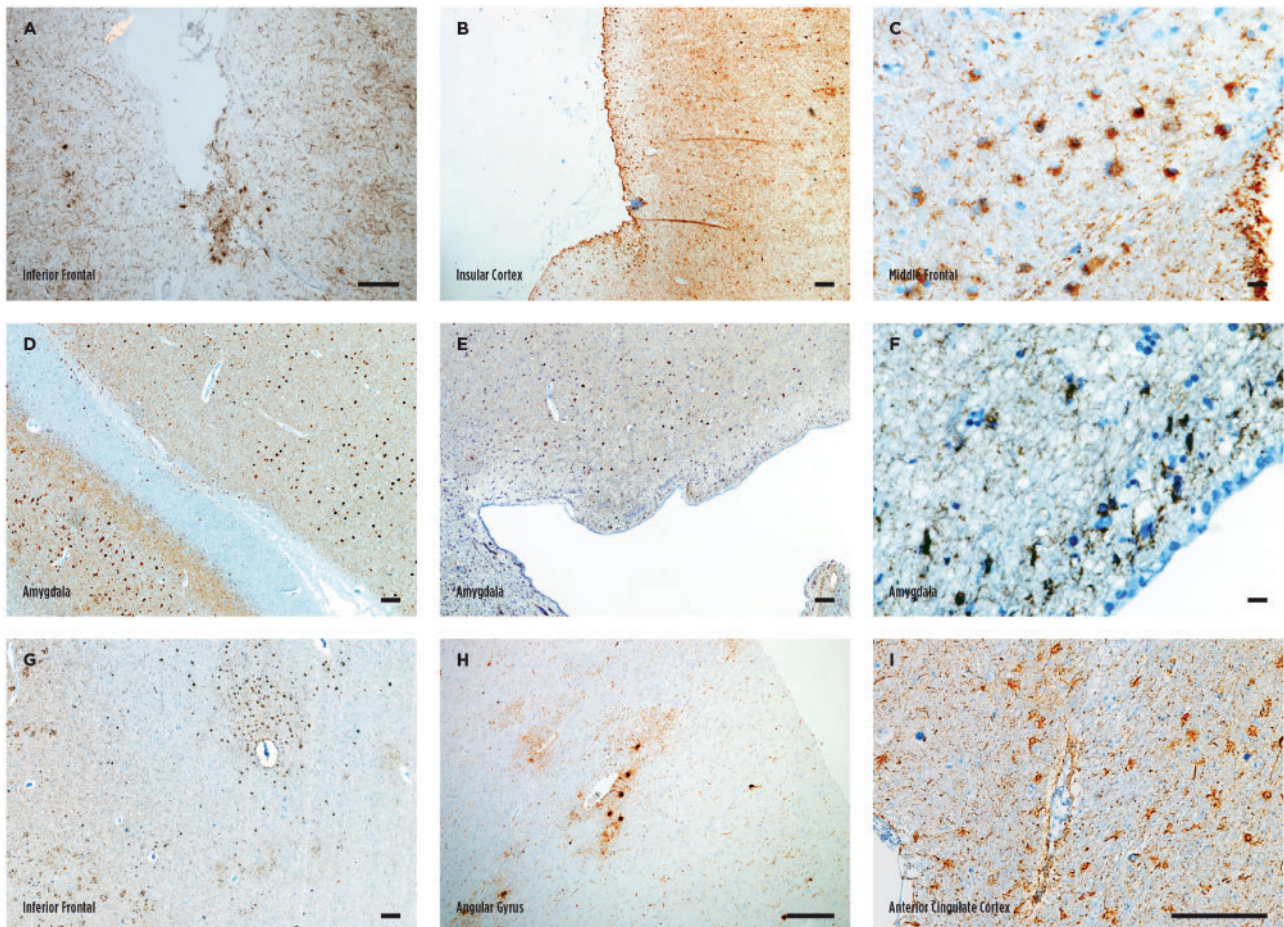


**FIGURE 2.** Subpial subependymal, and perivascular astrocytic tau deposition. **(A–C)** Representative images of subpial thorn-shaped astrocytes (TSA) visualized with phosphorylated tau immunostaining. A focal cluster at the sulcal depth is shown in **A**, while more diffuse deposition is shown in **B**. **(D–F)** Representative images of subependymal TSA in the amygdala. **(G–I)** Representative images of perivascular TSA in the cortex. Scale bars: **A, B, D, E, G–I**, 100  $\mu\text{m}$ ; **C and F**, 10  $\mu\text{m}$ .

one-way ANOVA, Fig. 3A). An analogous relationship was noted for both GFAs and TSAs in the grey matter ( $p = 0.49$  and  $p = 0.87$ , respectively, one-way ANOVA, Fig. 3B, C), although such pathologies were less frequent and occurred at lower densities than white matter/ATAC pathology.

In contrast, subpial accumulation of TSAs demonstrated a striking regional variation with the highest density occurring in the amygdala ( $p < 0.0001$ , one-way ANOVA, with all Tukey post hoc comparisons of amygdala deposition with every other area showing  $p < 0.05$ , Fig. 3D). Subependymal deposition also seemed to occur more frequently adjacent to the amygdala, at the anterior part of the inferior horn of the lateral ventricle, compared with other regions of the brain, but given the low numbers of cases with deposition outside the amygdala a significant increase in density was not observed ( $p = 0.08$ , one-way ANOVA, Fig. 3E). Finally, perivascular TSA deposition exhibited a differential distribution across regions ( $p < 0.05$ , one-way ANOVA, Fig. 3F) but significant differences between individual areas were not identified with post hoc analysis after correcting for multiple comparisons. The regions with a seemingly higher density occurred in

limbic regions as well as the putamen, rather than the cortical regions at the lateral convexities of the brain.

### Relationship Between ARTAG and Atypical Clinical Presentations of AD

Our extensive mapping of the ARTAG subtype distribution and density in key brain regions allowed us to investigate a possible association between ARTAG and an atypical cortical presentation of AD using both classical statistical modeling with multivariate linear regression as well as an unbiased clustering of pathological subtypes to evaluate for clinical significance.

We first built multivariate logistic regression models to evaluate how the presence of pathology throughout the brain and by subtype was related to clinical variables. The density and specific distribution of pathology were considered for the unbiased clustering analysis below. The independent variables included atypical clinical diagnosis (any case with a focal cortical presentation), age at death, sex, Braak stage, disease duration, *APOE4* carrier status, and the presence of AGD; while

**TABLE 2.** Pathological Findings by Clinical Diagnosis

| Clinical Diagnosis                               | Number | %<br>ARTAG | % White<br>Matter<br>TSA<br>(ATAC) | % Grey<br>Matter<br>TSA | % Grey<br>Matter<br>TSA at<br>Sulcal<br>Depth | % Grey<br>Matter<br>GFA | %<br>Subpial<br>TSA | %<br>Subpial<br>TSA<br>at Sulcal<br>Depth | %<br>Subependymal<br>TSA | %<br>Perivascular<br>TSA |
|--|--------|------------|------------------------------------|-------------------------|---|-------------------------|---------------------|---|--------------------------|--------------------------|
| Amnesic syndrome                                 | 46     | 67         | 57                                 | 24                      | 7   | 22                      | 41                  | 13  | 30                       | 30                       |
| Corticobasal syndrome                            | 7      | 43         | 43                                 | 14                      | 14  | 0                       | 14                  | 14  | 14                       | 14                       |
| p value  |        | 0.402      | 0.788                              | 0.934                   | 1.000   | 0.395                   | 0.339               | 1.000                                     | 0.665                    | 0.665                    |
| Behavioral variant<br>frontotemporal dementia    | 5      | 60         | 20                                 | 40                      | 0   | 20                      | 40                  | 0   | 60                       | 40                       |
| p value  |        | 1.000      | 0.279                              | 0.808                   | 1.000   | 1.000                   | 1.000               | 0.897                                     | 0.405                    | 1.000                    |
| Lewy Body Dementia                               | 1      | 100        | 0                                  | 0                       | 0   | 0                       | 0                   | 0   | 100                      | 0                        |
| p value  |        | —          | —                                  | —                       | —   | —                       | —                   | —   | —                        | —                        |
| Logopenic variant primary<br>progressive aphasia | 7      | 57         | 43                                 | 14                      | 14  | 0                       | 14                  | 0   | 29                       | 29                       |
| p value  |        | 0.916      | 0.788                              | 0.934                   | 1.000   | 0.395                   | 0.339               | 0.708                                     | 1.000                    | 1.000                    |
| Very mild dementia                               | 7      | 57         | 29                                 | 29                      | 0   | 43                      | 43                  | 14  | 43                       | 43                       |
| p value  |        | 0.916      | 0.330                              | 1.000                   | 1.000   | 0.460                   | 1.000               | 1.000                                     | 0.825                    | 0.825                    |
| Cognitively normal                               | 3      | 100        | 33                                 | 33                      | 0   | 67                      | 67                  | 0   | 100                      | 67                       |
| p value  |        | 0.589      | 0.855                              | 1.000                   | 1.000   | 0.289                   | 0.796               | 1.000                                     | 0.068                    | 0.508                    |
| Other  | 1      | 100        | 0                                  | 0                       | 0   | 0                       | 0                   | 0   | 100                      | 0                        |
| p value  |        | —          | —                                  | —                       | —   | —                       | —                   | —   | —                        | —                        |
| Posterior cortical atrophy                       | 6      | 50         | 50                                 | 17                      | 0   | 0                       | 33                  | 17  | 0                        | 17                       |
| p value  |        | 0.700      | 1.000                              | 1.000                   | 1.000   | 0.472                   | 1.000               | 1.000                                     | 0.275                    | 0.825                    |
| Total  | 83     | 64         | 47                                 | 23                      | 6   | 19                      | 36                  | 11  | 34                       | 30                       |

ARTAG, aging-related tau astroglipathy; ATAC, argyrophilic thorny astrocyte clusters; TSA, thorn shaped astrocyte; GFA, granular fuzzy astrocyte.

**TABLE 3.** Frequency of Co-occurring ARTAG Subtypes

|                                | % With White<br>Matter TSA (ATAC) | % With Grey<br>Matter TSA | % With<br>Grey Matter<br>GFA | % With<br>Subpial TSA | % With<br>Subependymal TSA | % With<br>Perivascular TSA |
|--------------------------------|-----------------------------------|---------------------------|------------------------------|-----------------------|----------------------------|----------------------------|
| <b>White matter TSA (ATAC)</b> | —                                 | 36                        | 31                           | 59                    | 49                         | 54                         |
| p value                        | —                                 | <b>0.017</b>              | <b>0.026</b>                 | <b>1.20e-4</b>        | <b>0.013</b>               | <b>2.72e-5</b>             |
| <b>Grey matter TSA</b>         | 74                                | —                         | 53                           | 79                    | 74                         | 79                         |
| p value                        | <b>0.017</b>                      | —                         | <b>1.11e-4</b>               | <b>3.31e-5</b>        | <b>8.93e-5</b>             | <b>5.79e-7</b>             |
| <b>Grey matter GFA</b>         | 75                                | 63                        | —                            | 94                    | 81                         | 81                         |
| p value                        | <b>0.026</b>                      | <b>1.11e-4</b>            | —                            | <b>4.45e-7</b>        | <b>2.92e-5</b>             | <b>3.19e-6</b>             |
| <b>Subpial TSA</b>             | 77                                | 50                        | 50                           | —                     | 73                         | 67                         |
| p value                        | <b>1.20e-4</b>                    | <b>3.31e-5</b>            | <b>4.45e-7</b>               | —                     | <b>3.82e-8</b>             | <b>1.88e-7</b>             |
| <b>Subependymal TSA</b>        | 68                                | 50                        | 46                           | 79                    | —                          | 71                         |
| p value                        | <b>0.013</b>                      | <b>8.93e-5</b>            | <b>2.92e-5</b>               | <b>3.82e-8</b>        | —                          | <b>2.15e-8</b>             |
| <b>Perivascular TSA</b>        | 84                                | 60                        | 52                           | 80                    | 80                         | —                          |
| p value                        | <b>2.72e-5</b>                    | <b>5.79e-7</b>            | <b>3.19e-6</b>               | <b>1.88e-7</b>        | <b>2.15e-8</b>             | —                          |

ATAC, argyrophilic thorny astrocyte clusters; TSA, thorn shaped astrocyte; GFA, granular fuzzy astrocyte.

the presence of ARTAG or its subtypes were considered as outcomes or dependent variables (Table 4). Age of death and Braak stage were the only significant variables to have an effect on the presence of ARTAG overall (p=0.003 and p=0.030, respectively, Table 4). Similar relationships with older age were observed for all subtypes, except grey matter TSA (p value range from 0.021 to 0.0004, Table 4).

Furthermore, Braak stage was also significantly associated with white matter/ATAC and subpial pathologies (p=0.012 and p=0.040, respectively, Table 4). While not associated with ARTAG as a whole, male sex was found to significantly relate to the presence of grey matter, subependymal and perivascular TSA pathology (p=0.024, p=0.008, p=0.033, respectively, Table 4). However, we failed to find any

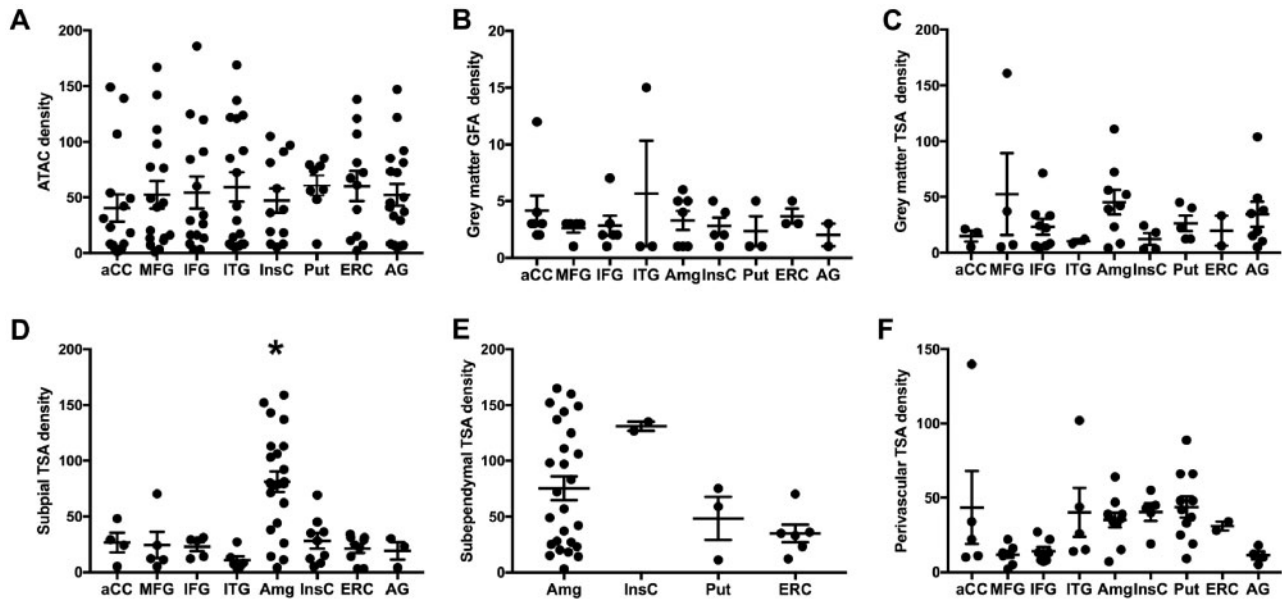


**FIGURE 3.** Anatomical distribution of astrocytic tau deposition by subtype and density. The cases with a nonzero density are plotted by region for argyrophilic thorny astrocyte clusters (ATAC)/white matter ARTAG (A), grey matter granular fuzzy astrocytes (GFA) (B), grey matter thorn-shaded astrocytes (TSA) (C), subpial TSA (D), subependymal TSA (E), and perivascular TSA (F). Each case with a nonzero density is represented with a symbol; solid lines indicate the mean and standard error of the mean. Asterisk indicates all Tukey post hoc comparisons of amygdala deposition with every other area ( $p < 0.05$ ).

**TABLE 4.** Multivariate Logistic Regression Analysis

| Variables          | ARTAG           | White Matter TSA (ATAC) | Grey Matter TSA | Grey Matter GFA  | Subpial TSA     | Subependymal TSA | Perivascular TSA |
|--------------------|-----------------|-------------------------|-----------------|------------------|-----------------|------------------|------------------|
| Atypical diagnosis | 0.15 (0.65)     | -0.26 (0.61)            | 0.06 (0.82)     | -19.06 (4043.27) | -1.24 (0.90)    | 0.63 (0.76)      | 0.68 (0.75)      |
| p value            | 0.818           | 0.662                   | 0.937           | 0.996            | 0.168           | 0.406            | 0.362            |
| Age of death       | 0.11 (0.04)     | 0.08 (0.03)             | 0.03 (0.04)     | 0.27 (0.12)      | 0.19 (0.05)     | 0.09 (0.04)      | 0.10 (0.04)      |
| p value            | <b>0.003</b>    | <b>0.008</b>            | 0.320           | <b>0.021</b>     | <b>0.0004</b>   | <b>0.013</b>     | <b>0.007</b>     |
| Male Sex           | 0.88 (0.57)     | -0.42 (0.56)            | 2.00 (0.89)     | 2.08 (1.49)      | 1.05 (0.83)     | 2.19 (0.82)      | 1.53 (0.72)      |
| p value            | 0.123           | 0.448                   | <b>0.024</b>    | 0.160            | 0.204           | <b>0.008</b>     | <b>0.033</b>     |
| Braak Stage        | 0.71 (0.33)     | 1.17 (0.46)             | -0.34 (0.30)    | -0.11 (0.45)     | 1.74 (0.85)     | 0.06 (0.29)      | 0.14 (0.28)      |
| p value            | <b>0.030</b>    | <b>0.012</b>            | 0.261           | 0.800            | <b>0.040</b>    | 0.842            | 0.634            |
| Disease Duration   | -0.13 (0.10)    | -0.04 (0.08)            | 0.13 (0.08)     | 0.35 (0.27)      | 0.16 (0.12)     | -0.09 (0.08)     | -0.08 (0.08)     |
| p value            | 0.196           | 0.625                   | 0.119           | 0.168            | 0.181           | 0.285            | 0.285            |
| APO_E Carrier      | 0.30 (0.60)     | -0.24 (0.56)            | -0.99 (0.70)    | -2.73 (1.66)     | -1.12 (0.82)    | -0.49 (0.65)     | -0.45 (0.63)     |
| p value            | 0.617           | 0.670                   | 0.155           | 0.010            | 0.171           | 0.493            | 0.475            |
| Presence of AGD    | 18.23 (1956.51) | 1.75 (1.29)             | 1.05 (1.02)     | 40.39 (8624.94)  | 21.25 (1821.94) | 2.04 (1.32)      | 1.03 (1.08)      |
| p value            | 0.993           | 0.174                   | 0.304           | 0.996            | 0.991           | 0.121            | 0.345            |

Coefficient (standard error); ARTAG, aging-related tau astroglipathy; ATAC, argyrophilic thorny astrocyte clusters; TSA, thorn shaped astrocyte; GFA, granular fuzzy astrocyte.

significant association between ARTAG or its subtypes and an atypical clinical diagnosis.

Next, we assessed how unbiased clustering of the cases, based on the density and distribution of pathology, might correlate with clinical variables. The data for all subtypes of pathology by location and density were included in the clustering analysis. Using a K-means algorithm, where the number of clusters was determined using a Cluster Validation

Package *clValid* in R and further evaluated by assessing Ward’s method of partitioning, we identified 3 pathological groups (Fig. 4). The first group was characterized by overall high densities of pathology throughout the brain and composed of 14 cases, the “high” group. The second group contained 52 cases which exhibited primarily low densities or no ARTAG pathology, the “low” group. Finally, the third group demonstrated prominent pathology surrounding the amygdala

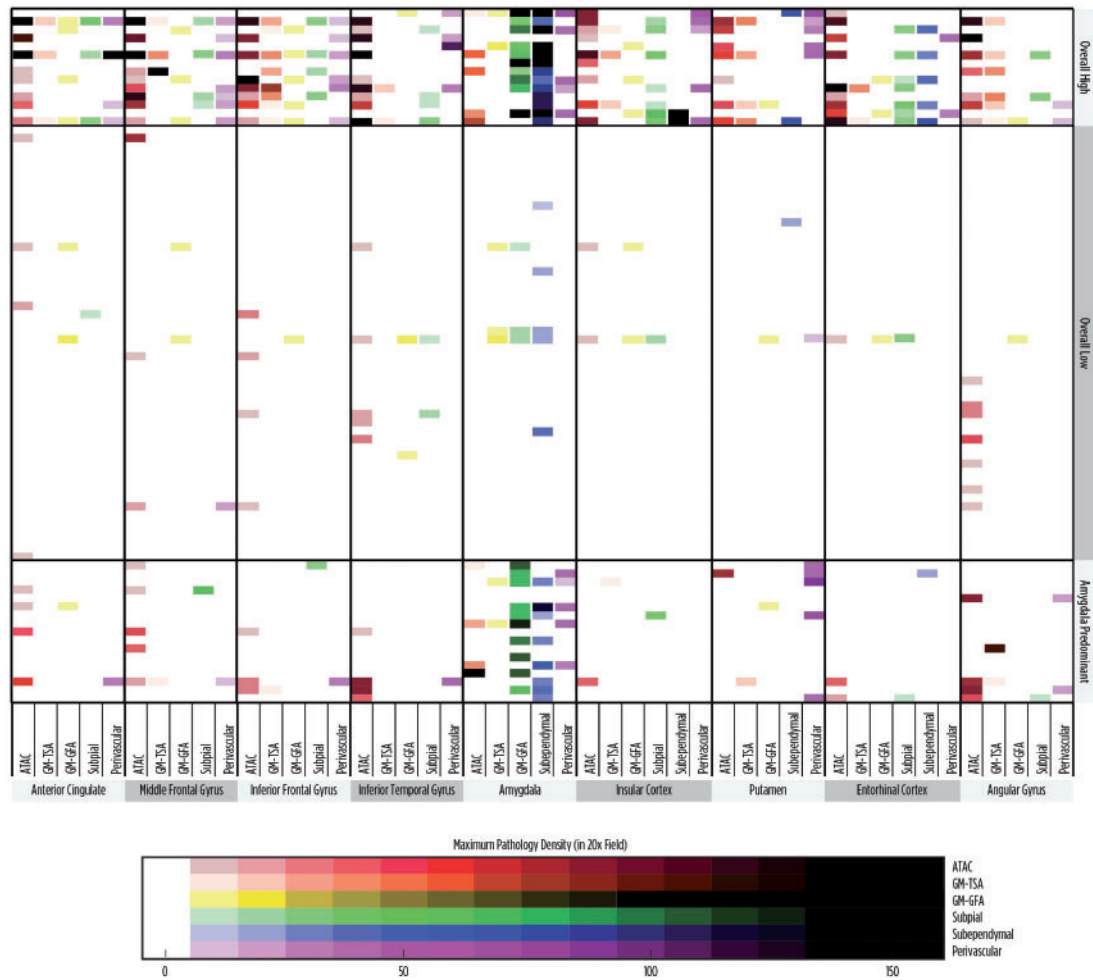


**FIGURE 4.** K-means clustering of cases by density and distribution of ARTAG pathology. Clustering analysis resulted in 3 significant groups with cases showing a high density of pathology throughout many regions, a low density or no pathology, or an amygdala-predominant pathology.

(n = 17, the “amygdala-predominant” group), with high densities of subependymal and/or subpial TSA deposition around the amygdala, while the cortical regions had relatively low levels of pathology. We further evaluated if these unbiased groupings of cases were associated with an atypical clinical diagnosis (Table 5), and no relationship was identified (p = 0.54, Chi-square test). In fact, the “high density” group had cases with classical amnesic syndrome as well atypical cases, including 2 cases of corticobasal syndrome and 1 case of a behavioral variant FTD-like syndrome. Similarly, the other low and amygdala-predominant groups had a mixture of amnesic and atypical cases. Despite the lack of association with an atypical syndrome, the clustering appeared to be biologically meaningful as sex and age were significantly different between groups (p = 0.028 and p = 0.0006; Chi-square test and Mann-Whitney U test, respectively). The distribution of ARTAG pathology subtypes is also shown by clinical diagnosis in Figure 5.

Since some studies of ARTAG distribution suggest an independent development of white matter TSA/ATAC pathology from other ARTAG subtypes (17), and an atypical clinical presentation (logopenic variant of primary progressive

aphasia) association has been noted specifically with ATAC pathology, we also evaluated the clustering of each subtype independently to ensure that any possible relationship to an atypical clinical presentation was not overlooked. All subtypes, except for subpial TSAs, clustered into 2 groups, demonstrating a high overall group versus a low to no pathology group. The subpial TSAs clustered into 3 groups that showed a similar pattern to the clustering of all types together: a high overall group, a low pathology group, and an amygdala-predominant group. Despite this additional clustering analysis, no relationship to an atypical clinical presentation was identified. The clustering for each subtype, along with the distribution of pathology for each subtype by clinical diagnosis, are presented in Supplementary Data Figures S1–S6. The demographics for each cluster by subtype are given in Supplementary Data Tables S1–S6.

## DISCUSSION

ARTAG is an umbrella term encompassing a broad array of age-associated tau inclusions in astrocytes. In this study

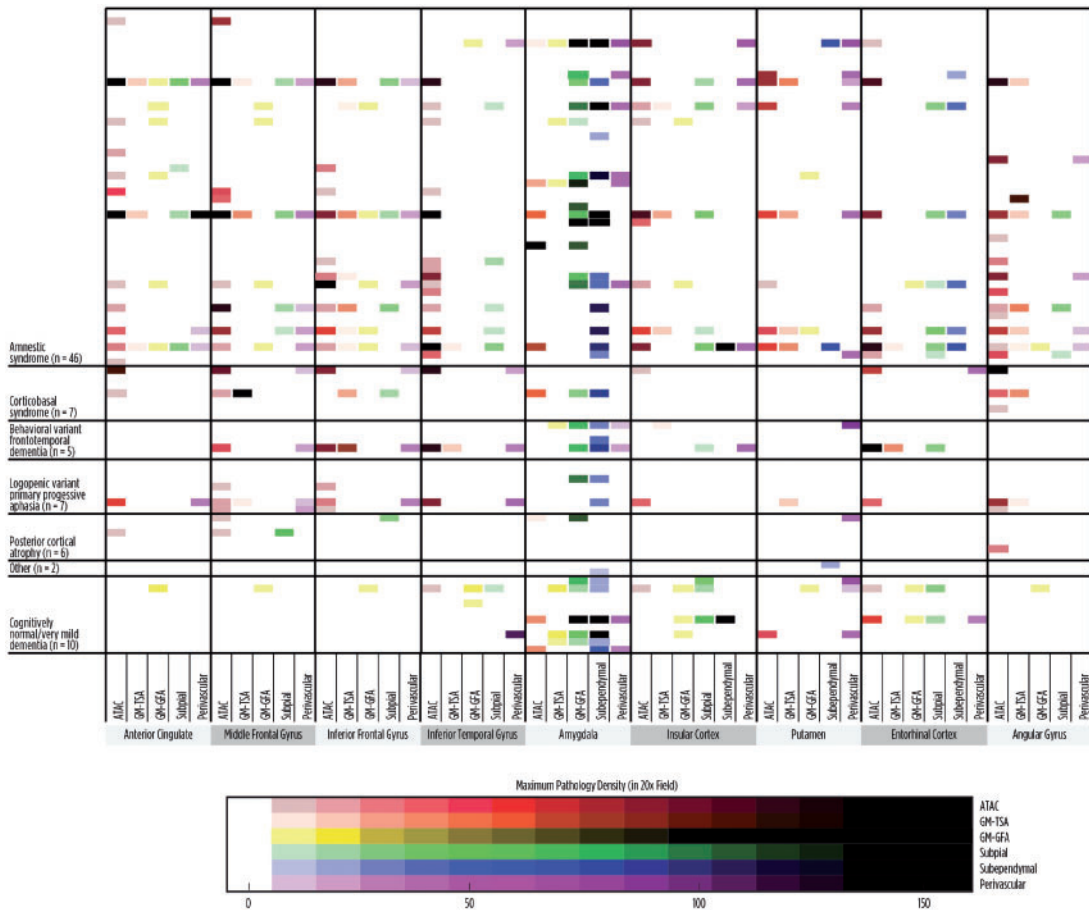


**FIGURE 5.** ARTAG density by clinical diagnosis. While many of the cases with a high and widespread ATAC density are noted in the classic AD group, several cases occur in the atypical clinical group, including cases with corticobasal syndrome and frontotemporal dementia-like syndrome.

**TABLE 5.** Demographics by ARTAG Clustering

| ARTAG Cluster        | Number | % Atypical | % Male       | Mean Age of Death (SD) | Mean Disease Duration (SD) | Mean Years of Education (SD) | %APOE4 Carrier | Median Braak NFT Stage |
|----------------------|--------|------------|--------------|------------------------|----------------------------|------------------------------|----------------|------------------------|
| Amygdala-predominant | 17     | 29         | 76           | 71.41 (8.66)           | 9.82 (5.02)                | 15.65 (3.53)                 | 56             | 6                      |
| Low                  | 52     | 37         | 52           | 69.94 (10.80)          | 9.38 (3.14)                | 15.51 (2.80)                 | 45             | 6                      |
| High                 | 14     | 21         | 86           | 82.57 (8.47)           | 9 (5.46)                   | 16.55 (5.71)                 | 31             | 6                      |
| p value              | —      | 0.325      | <b>0.028</b> | <b>0.0006</b>          | 0.993                      | 0.854                        | 0.447          | 0.493                  |

SD, standard deviation; NFT, neurofibrillary tangle.

of a large clinicopathological series of AD cases lacking any comorbid cortical pathologies, we assessed several cortical and subcortical regions and found that astrocytic tau deposition is frequent, is often correlated with older age, male sex, and Braak stage and the subtypes, defined by location and morphology, often co-occur. Furthermore, the distribution of pathology shows distinct patterns with subpial and subependymal deposition occurring prominently in the amygdala, while white matter ARTAG/ATAC and grey matter astrocytic deposition appear to be distributed throughout cortical regions without a particular lobar preference. Finally, we failed to find

a relationship either between the presence of ARTAG pathology or its subtypes or between one of the groups defined by unbiased clustering (high density, amygdala-predominant accumulation, or a low density of ARTAG pathology) and an atypical clinical presentation of AD.

Our findings are congruent with recent studies that have also mapped the patterns of ARTAG pathology in independent series with pure and mixed AD cases as well as primary tauopathies. In 2017, Kovacs et al identified a strikingly similar distribution of ARTAG and its subtypes in their cohort of AD/PART cases (n = 322) (38). ARTAG occurred overall in 63%

of their cases compared with 64% in our cohort. Also, 44% of their AD/PART cases showed white matter or ATAC pathology compared with 47% of our cases. The other subtypes exhibited a similar range between 20% and 40%. They found both focal and diffuse patterns of subpial, subependymal and white matter ARTAG within sections, and also noted that ARTAG subtypes were frequently found together. When specifically assessing the spatial distributions and possible sequential appearance of pathology for ARTAG in a subsequent paper (17), subpial and subependymal ARTAG were most frequently observed in the basal brain structures, such as the amygdala, similar to our data. However, it should be pointed out that our assessment of spatial distributions was broader, and we analyzed individual regions rather than grouping regions into 3 major areas: basal brain, lobar, and brainstem areas. Despite this difference in analysis and similar to our findings, Kovacs et al identified that white matter ARTAG pathology in the frontal, temporal, and parietal lobe appeared together in most cases. However, contrary to our findings, they concluded that the highest frequency of white matter ARTAG pathology occurred in the medial temporal lobe structures such as the amygdala. Part of the discrepancy with our results may be that almost all white matter pathology in the amygdala occurred in structures adjacent to the ependymal lining and was thus thought to represent an expansion of subependymal pathology into the white matter and categorized as subependymal ARTAG in our study. Similar to Forrest et al, sulcal accentuation of TSA pathology was also identified in our cohort, albeit at higher frequencies (12% overall compared with <2% in their study) and we did not find any pathology fulfilling CTE consensus criteria (39).

Logistic regression analysis to evaluate clinicopathologic correlations by Kovacs et al (38) also found that age and male sex were significantly associated with the overall presence of ARTAG, a finding previously reported in a cohort focusing on ARTAG deposition in the basal forebrain (13). When evaluating which variables were associated with different subtypes, they noted that white matter ARTAG, especially lobar white matter ARTAG was associated with AD-related variables including Braak stage, coinciding with our findings. A similar association of TSA and staging of neurofibrillary tangles has also been reported (40). While we identified that ARTAG subtypes frequently co-exist in the same brain, we did not specifically assess conditional probabilities within a specific region of the brain. With this conditional probability analysis, Kovacs et al suggest that the presence of frontal white matter ARTAG might be independent of subpial and grey matter ARTAG. Perhaps the differential presence and density of distribution for the ARTAG subtypes that we have found might also support this conclusion (17). Furthermore, the finding of the prominence of grey matter ARTAG within cortical sections evaluated in a community-based aging cohort compared with our finding of white matter predominant deposition in AD might also suggest an independent mechanism of disease (39).

In this more recent paper by Kovacs et al (2018), the authors also used unbiased clustering analysis (17). However, a direct comparison of results is not possible. Our analysis examined the quantitative density of all ARTAG pathologies or

each subtype independently throughout all sections examined, while their clustering algorithm analyzed the qualitative presence of subpial, white matter, and grey matter ARTAG all together throughout subregions of the brain. They found that cases with grey matter ARTAG cluster but failed to identify subgroups with differential distribution of other pathologies. Their use of qualitative data instead of quantitative density might explain this disagreement with our results.

In addition to the identification of similar patterns and distributions of ARTAG in comparison to the few previous investigations, our work brings novel insights. We are the first to carefully map ARTAG and its subtypes in cortical sections that are specific hubs of atrophy in cases of atypical AD presentations to investigate a possible role of ARTAG in clinical heterogeneity and regional atrophy. Nevertheless, we failed to find any association of the presence of ARTAG or its subtypes with atypical AD even when density and unbiased clustering were used to define the pathological groups. Previous studies have only included small numbers of cases with atypical presentations in their cohorts. Munoz et al. identified that white matter ARTAG/ATAC was present in 7/8 primary progressive aphasia with primary AD pathology and 0/6 amnesic AD cases (18). Subsequent reports noted frequent ATAC clusters in only 2/11 primary progressive aphasia, 1/10 FTD, and 2/27 classical amnesic AD cases (6, 41). We currently have found 10/27 atypical AD cases and 26/46 amnesic AD cases that contain white matter ARTAG/ATAC. Thus, ATAC is frequent and exists in cortical regions important in focal cortical presentations but does not seem to significantly occur more often in these cases. The relationship between other subtypes of ARTAG including subpial, grey matter, subependymal and perivascular and atypical AD presentations has not previously been evaluated, and we also have not identified any relationship with an atypical presentation for these subtypes with logistic regression analysis or unbiased clustering. It should be noted that while we have evaluated one of the largest cohorts to date of atypical clinical presentations of AD, the overall power of our study is limited by the number of cases and the heterogeneity of these atypical cases. Further studies with increased numbers of atypical cases are warranted to further investigate the presence of copathologies in these cases.

These results, however, do not necessarily imply that ARTAG is clinically irrelevant. Some have suggested an association with cognitive decline (19, 42), particularly with white matter ARTAG (38). Given our results of an association with age and Braak stage, one might postulate that white matter ARTAG accumulation might increase with disease progression and be more likely to affect symptoms later in the course of the disease rather than affecting the initial manifesting symptoms. Indeed, initial symptom onset is often part of the definition of atypical clinical syndromes such as primary progressive aphasia and the clinical diagnosis might not wholly encompass the patient's clinical function prior to death. Future studies are required to more fully investigate the nuances of how ARTAG effects function in different cognitive domains.

The finding of 3 pathological groups distinguished by a high-, low-, or amygdala-predominant density of ARTAG pathology and not by a differential anatomical distribution raises

intriguing questions about pathogenesis. Indeed, the lack of a similar distribution of 3R/4R tau-positive inclusions in astrocytes as found in neurofibrillary tangles might also suggest a separate mechanism of accumulation that cannot be purely attributed to phagocytosis of neuronal pathology (43). Does this imply a global response to injury at tissue interfaces throughout the brain rather than a specific network exhibiting selective vulnerability? The report of increased connexin-43 and aquaporin-4 expression with ARTAG (15) might further support this theory and highlight the relevance of further examination of the blood-brain barrier in this astroglial protein accumulation.

In summary, ARTAG deposition frequently co-occurs with AD regardless of a typical or atypical presentation. ARTAG distribution and density clusters into 3 types of cases: cases with low densities of pathology overall, cases with high densities throughout the brain, or cases having an amygdala-predominant deposition. Further research is needed to understand both the etiology of this deposition as well as the clinical significance for disease progression.

## REFERENCES

- Wu X, Li R, Fleisher AS, et al. Altered default mode network connectivity in Alzheimer's disease – A resting functional MRI and Bayesian network study. *Hum Brain Mapp* 2011;32:1868–81
- Lam B, Masellis M, Freedman M, et al. Clinical, imaging, and pathological heterogeneity of the Alzheimer's disease syndrome. *Alzheimers Res Ther* 2013;5:1
- de Souza LC, Bertoux M, Funkiewiez A, et al. Frontal presentation of Alzheimer's disease: A series of patients with biological evidence by CSF biomarkers. *Dement Neuropsychol* 2013;7:66–74
- Ossenkoppele R, Pijnenburg YA, Perry DC, et al. The behavioural/dysexecutive variant of Alzheimer's disease: Clinical, neuroimaging and pathological features. *Brain* 2015;138:2732–49
- Rohrer JD, Rossor MN, Warren JD. Alzheimer's pathology in primary progressive aphasia. *Neurobiol Aging* 2012;33:744–52
- Mesulam M, Wicklund A, Johnson N, et al. Alzheimer and frontotemporal pathology in subsets of primary progressive aphasia. *Ann Neurol* 2008;63:709–19
- Lee SE, Rabinovici GD, Mayo MC, et al. Clinicopathological correlations in corticobasal degeneration. *Ann Neurol* 2011;70:327–40
- Crutch SJ, Lehmann M, Schott JM, et al. Posterior cortical atrophy. *Lancet Neurol* 2012;11:170–8
- Hassan A, Whitwell JL, Josephs KA. The corticobasal syndrome-Alzheimer's disease conundrum. *Expert Rev Neurother* 2011;11:1569–78
- Nelson PT, Alafuzoff I, Bigio EH, et al. Correlation of Alzheimer disease neuropathologic changes with cognitive status: A review of the literature. *J Neuropathol Exp Neurol* 2012;71:362–81
- Tang-Wai DF, Josephs KA, Boeve BF, et al. Coexistent Lewy body disease in a case of “visual variant of Alzheimer's disease”. *J Neurol Neurosurg Psychiatry* 2003;74:389
- Kovacs GG, Ferrer I, Grinberg LT, et al. Aging-related tau astroglial pathology (ARTAG): Harmonized evaluation strategy. *Acta Neuropathol* 2016;131:87–102
- Liu AK, Goldfinger MH, Questari HE, et al. ARTAG in the basal forebrain: Widening the constellation of astrocytic tau pathology. *Acta Neuropathol Commun* 2016;4:59
- Kovacs GG, Xie SX, Lee EB, et al. Multisite assessment of aging-related tau astroglial pathology (ARTAG). *J Neuropathol Exp Neurol* 2017;76:605–19
- Kovacs GG, Yousef A, Kaindl S, et al. Connexin-43 and aquaporin-4 are markers of ageing-related tau astroglial pathology (ARTAG)-related astroglial response. *Neuropathol Appl Neurobiol* 2018;44:491–505
- Ferrer I, Garcia MA, Gonzalez IL, et al. Aging-related tau astroglial pathology (ARTAG): Not only tau phosphorylation in astrocytes. *Brain Pathol* 2018;28:965–85.
- Kovacs GG, Xie SX, Robinson JL, et al. Sequential stages and distribution patterns of aging-related tau astroglial pathology (ARTAG) in the human brain. *Acta Neuropathol Commun* 2018;6:50
- Munoz DG, Woulfe J, Kertesz A. Argyrophilic thorny astrocyte clusters in association with Alzheimer's disease pathology in possible primary progressive aphasia. *Acta Neuropathol* 2007;114:347–57
- Robinson JL, Corrada MM, Kovacs GG, et al. Non-Alzheimer's contributions to dementia and cognitive resilience in The 90+ Study. *Acta Neuropathol* 2018;136:377–88
- Cairns NJ, Bigio EH, Mackenzie IR, et al. Neuropathologic diagnostic and nosologic criteria for frontotemporal lobar degeneration: Consensus of the Consortium for Frontotemporal Lobar Degeneration. *Acta Neuropathol* 2007;114:5–22
- Dickson DW, Bergeron C, Chin SS, et al. Office of Rare Diseases neuropathologic criteria for corticobasal degeneration. *J Neuropathol Exp Neurol* 2002;61:935–46
- McKeith IG, Dickson DW, Lowe J, et al. Diagnosis and management of dementia with Lewy bodies: Third report of the DLB Consortium. *Neurology* 2005;65:1863–72
- Montine TJ, Phelps CH, Beach TG, et al. National Institute on Aging-Alzheimer's Association guidelines for the neuropathologic assessment of Alzheimer's disease: A practical approach. *Acta Neuropathol* 2012;123:1–11
- Hauw JJ, Daniel SE, Dickson D, et al. Preliminary NINDS neuropathologic criteria for Steele-Richardson-Olszewski syndrome (progressive supranuclear palsy). *Neurology* 1994;44:2015–9
- Mackenzie I, Neumann M, Bigio E, et al. Nomenclature and nosology for neuropathologic subtypes of frontotemporal lobar degeneration: An update. *Acta Neuropathol* 2010;119:1–4
- Mackenzie IR, Neumann M, Baborie A, et al. A harmonized classification system for FTLTDP pathology. *Acta Neuropathol* 2011;122:111–3
- Ferrer I, Santpere G, van Leeuwen FW. Argyrophilic grain disease. *Brain* 2008;131:1416–32
- Rodriguez RD, Grinberg LT. Argyrophilic grain disease: An underestimated tauopathy. *Dement Neuropsychol* 2015;9:2–8
- Rodriguez RD, Suemoto CK, Molina M, et al. Argyrophilic Grain Disease: Demographics, clinical, and neuropathological features from a large autopsy study. *J Neuropathol Exp Neurol* 2016;75:628–35
- McKhann G, Drachman D, Folstein M, et al. Clinical diagnosis of Alzheimer's disease: Report of the NINCDS-ADRDA Work Group under the auspices of Department of Health and Human Services Task Force on Alzheimer's Disease. *Neurology* 1984;34:939–44
- McKhann GM, Knopman DS, Chertkow H, et al. The diagnosis of dementia due to Alzheimer's disease: Recommendations from the National Institute on Aging-Alzheimer's Association workgroups on diagnostic guidelines for Alzheimer's disease. *Alzheimers Dement* 2011;7:263–9.
- Dubois B, Feldman HH, Jacova C, et al. Advancing research diagnostic criteria for Alzheimer's disease: The IWG-2 criteria. *Lancet Neurol* 2014;13:614–29.
- Crutch SJ, Schott JM, Rabinovici GD, et al. Consensus classification of posterior cortical atrophy. *Alzheimers Dement* 2017;13:870–84.
- Gorno-Tempini ML, Hillis AE, Weintraub S, et al. Classification of primary progressive aphasia and its variants. *Neurology* 2011;76:1006–14
- Armstrong MJ, Litvan I, Lang AE, et al. Criteria for the diagnosis of corticobasal degeneration. *Neurology* 2013;80:496–503
- Rascovsky K, Hodges JR, Knopman D, et al. Sensitivity of revised diagnostic criteria for the behavioural variant of frontotemporal dementia. *Brain* 2011;134:2456–77
- Neary D, Snowden JS, Gustafson L, et al. Frontotemporal lobar degeneration: A consensus on clinical diagnostic criteria. *Neurology* 1998;51:1546–54
- Kovacs GG, Robinson JL, Xie SX, et al. Evaluating the patterns of aging-related tau astroglial pathology unravels novel insights into brain aging and neurodegenerative diseases. *J Neuropathol Exp Neurol* 2017;76:270–88
- Forrest SL, Kril JJ, Wagner S, et al. Chronic traumatic encephalopathy (CTE) is absent from a European community-based aging cohort while cortical aging-related tau astroglial pathology (ARTAG) is highly prevalent. *J Neuropathol Exp Neurol* 2019;78:398–405

40. Wharton SB, Minett T, Drew D, et al. Epidemiological pathology of Tau in the ageing brain: Application of staging for neuropil threads (BrainNet Europe protocol) to the MRC cognitive function and ageing brain study. *Acta Neuropathol Commun* 2016;4:11
41. Bigio EH, Mishra M, Hatanpaa KJ, et al. TDP-43 pathology in primary progressive aphasia and frontotemporal dementia with pathologic Alzheimer disease. *Acta Neuropathol* 2010;120:43–54
42. Kovacs GG, Molnar K, Laszlo L, et al. A peculiar constellation of tau pathology defines a subset of dementia in the elderly. *Acta Neuropathol* 2011;122:205–22
43. Okamoto K, Amari M, Fukuda T, et al. Astrocytic tau pathologies in aged human brain. *Neuropathology* 2019;39:187–93